

Adaptive Detection of Dim Maneuvering Targets in Adjacent Range Cells

Sheng Yan, Pia Addabbo, *Senior Member, IEEE*, Chengpeng Hao, *Senior Member, IEEE*, and Danilo Orlando, *Senior Member, IEEE*

Abstract—This letter addresses the detection problem of dim maneuvering targets in the presence of range cell migration. Specifically, it is assumed that the moving target can appear in more than one range cell within the transmitted pulse train. Then, the Bayesian information criterion and the generalized likelihood ratio test design procedure are jointly exploited to come up with six adaptive decision schemes capable of estimating the range indices related to the target migration. The computational complexity of the proposed detectors is also studied and suitably reduced. Simulation results show the effectiveness of the newly proposed solutions also for a limited set of training data and in comparison with suitable counterparts.

Index Terms—Adaptive detection, dim maneuvering targets, range cell migration, radar, sonar, Model Order Selection rules, generalized likelihood ratio test.

I. INTRODUCTION

ADAPTIVE detection is a task of primary concern in radar and sonar systems [1], [2]. As a matter of fact, in the last decades, a large number of architectures have been developed for the detection of target echoes competing against noise and clutter interference by means of array of sensors. The common aspect for most of these contributions is the assumption that the target is point-like and located in the cell under test (CUT) only at a given range.

However, there exist at least three cases where the above assumption may be no longer valid. Specifically, the first situation concerns high-resolution radars [3] and sonars [4] which can resolve a target into several scattering centers occupying several consecutive range cells. In fact, a large amount of detection algorithms for range-spread target can be found in the open literature (see [3]–[7] and references therein).

The second case is related to the spillover of target energy between consecutive matched filter samples which makes a point-like target extended in range [8] yielding a detection performance degradation when only one sample is processed. In the seminal paper [9], the authors propose a detection architecture that jointly processes adjacent range cells to take advantage of the spillover limiting the aforementioned degradation.

This work was in part supported by the National Natural Science Foundation of China under Grant 61971412.

Sheng Yan and Chengpeng Hao are with Institute of Acoustics, Chinese Academy of Sciences, Beijing, China (e-mail: yansheng@mail.ioa.ac.cn; haochengp@mail.ioa.ac.cn).

Pia Addabbo is with the Università degli Studi “Giustino Fortunato,” 82100 Benevento, Italy (e-mail: p.addabbo@unifortunato.eu).

Daniilo Orlando is with the Università degli Studi “Niccolò Cusano,” 00166 Roma, Italy (e-mail: daniilo.orlando@unicusano.it).

The third situation arises from the need of increasing the signal-to-interference-plus-noise ratio (SINR) in the case of dim targets to guarantee reliable detection performance and high-quality target parameter estimates. To this end, radar systems transmit long bursts of pulses and integrate the corresponding backscattered energy. However, dim maneuvering targets can move through more than one range cell within the integration time interval [10]. As a consequence, it prevents conventional decision schemes from exploiting all the backscattered energy, since they are fed by the range bin under test only and, hence, do not account for the target migration to the contiguous range bin. Therefore, methods to cope with range cell migration (RCM) become of primary importance. A widely used tool for RCM compensation is the Keystone transform which has been applied in several fields as, for instance, radar detection [10] to mitigate target RCM due to radial velocity and acceleration, synthetic aperture radar imaging [11], [12] where the RCM is caused by linear range walk and range curvature. In [13], an alternative method relying on adjacent correlation function and Lv’s transform is devised to detect the maneuvering targets with radial jerk motion. More recently, in [14], innovative one-step and two-step detection architectures are conceived for dim maneuvering targets with and without estimating the slow-time index of the target signal in the CUT and based upon the generalized information criterion [15]. Remarkably, such architectures can overcome conventional detectors as the generalized adaptive matched filter (GAMF) [16] at the price of an increased computational complexity.

In this letter, we focus on the detection of dim maneuvering targets in the presence of RCM and further improve the results of [14] by devising innovative robust (with respect to the amount of training samples) architectures. To this end, we do not consider any possible phase/amplitude relationships between consecutive pulses and exploit, at the design stage, the Bayesian information criterion (BIC) rule [15], which is an asymptotic approximation of the optimal maximum a posteriori rule, to identify the pulse echoes containing target components over two consecutive range cells. Then, we conceive two-step architectures (TSA) and one-step architectures (OSA) relying on GLRT-based design criteria, where GLRT stands for generalized likelihood ratio test. The contributions of the present letter can be summarized as follows: 1) unlike [14], all the samples from two consecutive range cells occupied by the target are processed to increase the detection performance; 2) the samples free of signal components are exploited for the estimation of the interference covariance

matrix (ICM) lending new architectures a robustness to the training set size; 3) the proposed architectures are designed to avoid a continuous computation of inverse matrices saving computational resources.

The letter is organized as follows: Section II contains the system model and the problem formulation. In Section III, TSAs and OSAs are devised including suitable modifications of them. Section IV is devoted to the numerical analysis and discussion. Finally, Section V concludes this letter outlining future research tracks.

II. SYSTEM MODEL AND PROBLEM STATEMENT

Let¹ us consider a (radar or sonar) system equipped with a linear array of N_a identical and uniformly distributed sensors (the inter-element spacing d is half of the operating wavelength, λ say, to avoid spatial aliasing). Moreover, denote by N_p pulses belonging to the transmitted pulse train. Then, for a point-like target, the signal received by the m th antenna element can be written as [14]

$$x_m(t) = \Re \left\{ \alpha \sum_{n=0}^{N_p-1} p\left(t - nT - \tau_0 + \frac{2v_t}{c}nT\right) \times e^{j2\pi(f_c+f_d)t} e^{j2\pi(m-1)\nu_s} \right\}, \quad (1)$$

where $\alpha \in \mathbb{C}$ accounts for target and channel effects, $T > 0$ is the pulse repetition time (PRT), $p(t)$ is an unit-energy pulse waveform, τ_0 is the round-trip delay of the target, v_t is the target radial velocity, c is the waveform velocity of propagation, f_c is the carrier frequency, f_d is the target Doppler frequency, and $\nu_s = \frac{d \cos \psi}{\lambda}$ is the spatial frequency with ψ the nominal target angle of arrival (AOA). After matched filtering and digital sampling, for the q th range cell (fast time) which is the target location at $t = 0$ we obtain the data sequence as [9]

$$y_m(q, g) = \alpha e^{j2\pi f_d T(g-1)} \mathcal{X}_p(\tau_0 - (g-1)T_p) + (g-1) \frac{2v_t}{c} T, f_d e^{j2\pi(m-1)\nu_s} \triangleq \alpha(q, g) e^{j2\pi(m-1)\nu_s}, \quad (2)$$

where $g \in \Omega_p = \{1, \dots, N_p\}$ indexes the slow time, $(g-1) \frac{2v_t}{c} T$ accounts for the range migration, $\mathcal{X}_p(\cdot, \cdot)$ is the ambiguity function of $p(t)$, T_p is the one-sided mainlobe width of the zero-Doppler cut of \mathcal{X}_p , and $\alpha(q, g) = \alpha e^{j2\pi f_d T(g-1)} \mathcal{X}_p(\tau_0 - (g-1)T_p + (g-1) \frac{2v_t}{c} T, f_d)$. Equation (2) highlights that, in the case of maneuvering targets and for large values of g (and, hence, of N_p), target response (ambiguity function value) associated with the q th range bin can decrease to zero implying that the mainlobe of the ambiguity function has migrated to the next contiguous range

¹Notation: In what follows, vectors and matrices are denoted by boldface lower-case and upper-case letters, respectively. $(\cdot)^\dagger$, $(\cdot)^T$, and $\det(\cdot)$ denote the complex conjugate transpose, the transpose, and the determinant, respectively, of the matrix argument, whereas the imaginary unit is j . As to the numerical sets, \mathbb{C} is the set of complex numbers, and $\mathbb{C}^{N \times M}$ is the Euclidean space of $(N \times M)$ -dimensional complex matrices (or vectors if $M = 1$). The symbol $\Re\{\cdot\}$ indicates the real part of a complex number, and the symbol \triangleq denotes a definition. The i th entry of a vector \mathbf{x} is indicated by $\mathbf{x}(i)$ and $\mathbf{0}$ denotes the null vector whose size depends on the the context. Finally, we write $\mathbf{x} \sim \mathcal{CN}_N(\mathbf{m}, \mathbf{M})$ if \mathbf{x} is a complex circular N -dimensional normal vector with mean \mathbf{m} and positive definite covariance matrix \mathbf{M} .

bin, namely the RCM has occurred. In what follows, for simplicity and without loss of generality, we set $q = 1$ and, hence, the next contiguous range bin is indexed by $q = 2$. Now, let us define by $\mathbf{Z}_i = [\mathbf{z}_{i,1}, \mathbf{z}_{i,2}, \dots, \mathbf{z}_{i,N_p}] \in \mathbb{C}^{N_a \times N_p}$, $i = 1, 2$, the data matrix corresponding to the i th range bin whose columns contain the returns from the N_a spatial channels. Then, if we assume that the \bar{g} th echo from range bin 1 contains target components and that the same echo from range bin 2 is representative of interference only, we can write $\mathbf{z}_{1,\bar{g}} = [y_1(1, \bar{g}), \dots, y_{N_a}(1, \bar{g})]^T + \mathbf{n}_{1,\bar{g}} \triangleq \alpha(1, \bar{g})\mathbf{v} + \mathbf{n}_{1,\bar{g}}$ and $\mathbf{z}_{2,\bar{g}} = \mathbf{n}_{2,\bar{g}}$, where $\mathbf{v} = [1, e^{j2\pi\nu_s}, \dots, e^{j2\pi(N_a-1)\nu_s}]^T \in \mathbb{C}^{N_a \times 1}$ is the nominal spatial steering vector depending on ψ and the $\mathbf{n}_{i,g}$ s are the interference components. When the RCM occurs for some pulse index \bar{g} , previous situation changes, namely $\mathbf{z}_{1,\bar{g}} = \mathbf{n}_{1,\bar{g}}$ is representative of interference only whereas $\mathbf{z}_{2,\bar{g}} = \alpha(2, \bar{g})\mathbf{v} + \mathbf{n}_{2,\bar{g}}$ also contains target components. A pictorial description of the RCM is shown in Fig. 1, where the blue squares denote data with target components and white squares denote data free of useful signal echoes. In the first l pulses, the target is in the first cell, then, it moves to the second range cell.

Therefore, in order to account for possible range migration, it is reasonable to process the returns associated with (at least) two consecutive range cells. Summarizing, the detection problem at hand can be formulated in terms of the following multiple hypothesis test

$$\left\{ \begin{array}{l} H_{l,h} : \left\{ \begin{array}{l} \mathbf{z}_{1,l+1} = \mathbf{n}_{1,l+1}, \dots, \mathbf{z}_{1,N_p} = \mathbf{n}_{1,N_p}, \\ \mathbf{z}_{2,1} = \mathbf{n}_{2,1}, \dots, \mathbf{z}_{2,l} = \mathbf{n}_{2,l}, \\ \mathbf{z}_{2,l+h+1} = \mathbf{n}_{2,l+h+1}, \dots, \\ \mathbf{z}_{2,N_p} = \mathbf{n}_{2,N_p}, \\ \mathbf{z}_{1,1} = \alpha(1, 1)\mathbf{v} + \mathbf{n}_{1,1}, \dots, \\ \mathbf{z}_{1,l} = \alpha(1, l)\mathbf{v} + \mathbf{n}_{1,l}, \\ \mathbf{z}_{2,l+1} = \alpha(2, l+1)\mathbf{v} + \mathbf{n}_{2,l+1}, \dots, \\ \mathbf{z}_{2,l+h} = \alpha(2, l+h)\mathbf{v} + \mathbf{n}_{2,l+h}, \\ \mathbf{r}_k = \mathbf{m}_k, k = 1, \dots, K, \end{array} \right. \\ H_0 : \left\{ \begin{array}{l} \mathbf{z}_{1,1} = \mathbf{n}_{1,1}, \dots, \mathbf{z}_{1,N_p} = \mathbf{n}_{1,N_p}, \\ \mathbf{z}_{2,1} = \mathbf{n}_{2,1}, \dots, \mathbf{z}_{2,N_p} = \mathbf{n}_{2,N_p}, \\ \mathbf{r}_k = \mathbf{m}_k, k = 1, \dots, K, \end{array} \right. \end{array} \right. \quad (3)$$

where $\mathbf{R} = [\mathbf{r}_1 \dots \mathbf{r}_K]$ are the training data, $1 \leq l \leq N_p$, $0 \leq h \leq N_p - l$ are unknown integers indexing which vectors contain target components, $\mathbf{n}_{1,i}, \mathbf{n}_{2,i}, \mathbf{m}_i \sim \mathcal{CN}_{N_a}(\mathbf{0}, \mathbf{M})$ are statistically independent interference vectors. As for $\alpha(1, i), i = 1, \dots, l$ and $\alpha(2, i), i = l+1, \dots, l+h$, they are modeled according to the Swerling II model [17]. Finally, note that when $H_{l,h}$ is declared, the nominal target AOA ψ can be used as a preliminary estimate of the actual target AOA.

III. DESIGN ISSUES

In this section, we devise two classes of architectures for problem (3). The first class pursues a natural approach which consists in estimating the pulse indices corresponding to the range transition (Subsection III.A) and then in applying decision schemes based upon such estimates (Subsection III.B). It follows that such architectures consist of two stages (TSA): the first stage solves the RCM problem whereas the second stage is responsible for target detection. The second approach (OSA)

incorporated into the decision statistic. This first architecture (OSA-1) relies on the GAMF [16] and is given by

$$\max_{\substack{l \in \Omega_p \\ h: l+h \leq N_p}} \left\{ \Lambda_{l,h}(\mathbf{Z}, \mathbf{S}) - \frac{p_1(l, h)}{2K} \right\} \underset{H_0}{\overset{H_{l,h}}{\geq}} \eta. \quad (11)$$

The second architecture (OSA-2) is obtained by applying the logarithm of the GLRT over both primary and secondary data, namely

$$\begin{aligned} \max_{\substack{l \in \Omega_p \\ h: l+h \leq N_p}} \left\{ \ln[f(\mathbf{R}; \hat{\mathbf{M}}_{l,h}) f_{l,h}(\mathbf{Z}; \hat{\alpha}_l, \hat{\mathbf{M}}_{l,h})] - \frac{p_2(l, h)}{2} \right\} \\ - \max_{\mathbf{M}} \left\{ \ln[f(\mathbf{R}; \mathbf{M}) f_0(\mathbf{Z}; \mathbf{M})] \right\} \underset{H_0}{\overset{H_{l,h}}{\geq}} \eta, \quad (12) \end{aligned}$$

where $f_0(\mathbf{Z}; \mathbf{M})$ is the PDF of \mathbf{Z} under H_0 . It is possible to show that (12) can be recast as

$$\ln \det \left(\frac{\mathbf{S} + \mathbf{Z}\mathbf{Z}^\dagger}{2N_p + K} \right) + \max_{\substack{l \in \Omega_p \\ h: l+h \leq N_p}} \left(\ln \frac{1}{\det(\hat{\mathbf{M}}_{l,h})} - \frac{p_2(l, h)}{(4N_p + 2K)} \right) \underset{H_0}{\overset{H_{l,h}}{\geq}} \eta. \quad (13)$$

IV. PERFORMANCE ASSESSMENT

In this section, we investigate the behavior of the proposed architectures in terms of probability of detection (P_d), computational complexity, and mean value of misclassified pulses (MVMP) defined as the sum of the number of pulses containing target components but classified as noise and the number of noise-only pulses classified as target (this metric is estimated only for the TSAs since OSAs inherit the selection capabilities of BIC). The competitors are the likelihood ratio test assuming perfect knowledge of l , h , and \mathbf{M} (clairvoyant detector), the GAMF and the generalized adaptive subspace detector (GASD) [16] both over data from two range cells, and the best detector of [14] defined by (10) and (11) (2S-GIC) and fed by data from the first range bin. Notice that the clairvoyant detector represents an upper bound for the performance.

The parameters of the high-resolution radar and maneuvering target are: $f_c = 10.0$ GHz, bandwidth 500 MHz, range resolution 0.3 m, PRT = 1 ms, $N_p = 16$, $N_a = 8$ and $v_t = 30$ m/s. In this scenario, the point-like target will occupy more than one range cell during a pulse integration interval. The related curves of P_d versus SINR (defined as in [14]) for $P_{fa} = 10^{-3}$, $K = 12 < 2N_a$ are shown in Fig. 2(a). It turns out that M-TSA-1 overcomes the other competitors with a gain of more than 9 dB over the GAMF at $P_d > 0.5$. The TSA-2, OSA-2, and M-TSA-2 follow the M-TSA-1 and with P_d values contained in an interval of about 1 dB. The 2S-GIC experiences a loss of 4 dBs with respect to M-TSA-2. The MVMP curves versus SINR are shown in Fig. 2(b). Inspection of the figure highlights that for SINR values lower than 10 dB, architectures based on (5) return better estimation results than TSA-2 (rule (7)) and M-TSA-2 (rule (8)). When $\text{SINR} > 10$ dB values, (7) and (8) slightly outperform (5). The detection performances when the RCM does not occur are shown in Fig. 2(c) for $P_{fa} = 10^{-3}$, $K = 12$, $l = N_p$, and $h = 0$. The M-TSA-1 still guarantees superior performance over the other detectors.

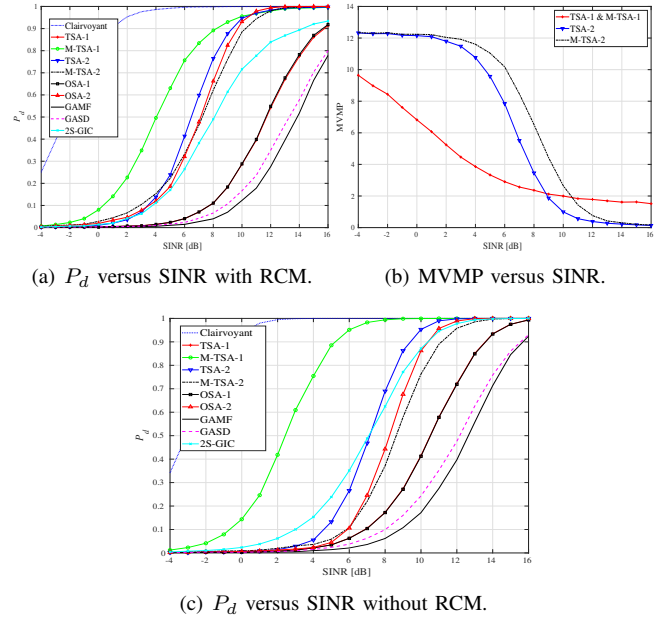


Fig. 2. Detection and estimation performance.

Finally, we compare the considered architectures from a computational point of view using the usual Landau notation. As expected, the GAMF is the architecture with the lowest computational load since it does not involve the determinant computation, data-dependent normalization, and discrete search; its computational load is given by $\mathcal{O}(N_a^3 + N_a^2 K + 2N_a N_p)$. The GASD with complexity $\mathcal{O}(N_a^3 + N_a^2(K + 2N_p))$ is slightly more time demanding than the GAMF due to the data-dependent normalization and shares a similar complexity with OSA-1 and TSA-1, that, in turn, are $\mathcal{O}(N_a^3 + N_a^2 K + 2N_a N_p + \frac{1}{2} N_p^2)$. Proceeding in order of increasing complexity, we obtain that M-TSA-1 and M-TSA-2 are $\mathcal{O}(2N_a^3 + N_a^2(K + 2N_p))$ and $\mathcal{O}(\frac{1}{2} N_a^3 N_p^2 + \frac{3}{2} N_a^2 N_p^2)$, respectively. The most complex architectures are OSA-2 and TSA-2, which are $\mathcal{O}(N_a^3 N_p^2 + 2N_a^2 N_p^2 + N_a N_p^3)$, and 2S-GIC whose complexity is $\mathcal{O}(N_a^3 N_p^2 + \frac{3}{2} N_a^2 N_p^2 + \frac{1}{2} N_a N_p^3)$. As a matter of fact, they require the computation of $\hat{\mathbf{M}}_{l,h}$ and its determinant for each $l \in \Omega_p$ and $h: l+h \leq N_p$. Summarizing, the analysis singles out the M-TSA-1 as the architecture that provides an excellent compromise between detection/estimation performance and computational load.

V. CONCLUSION

This letter focused on the adaptive detection of dim maneuvering target in the presence of range migration. In this context, data containing the returns from two adjacent range cells have been exploited to conceive six different decision schemes with different computational requirements that incorporate the BIC rule to estimate the range migration indices. The performance assessment pointed out that the M-TSA-1 can ensure an excellent trade off between detection performance and computational cost also for low volumes of training data. Future research tracks may include the design of architectures accounting for the spillover of target energy or heterogeneous environments.

REFERENCES

- [1] F. Bandiera, D. Orlando, and G. Ricci, *Advanced Radar Detection Schemes Under Mismatched Signal Models*. San Rafael, US: Synthesis Lectures on Signal Processing No. 8, Morgan & Claypool Publishers, 2009.
- [2] X. R. Li and V. P. Jilkov, "The generalized sinusoidal frequency-modulated waveform for active sonar," *IEEE Journal of Oceanic Engineering*, vol. 42, no. 1, pp. 109–123, Jan. 2017.
- [3] J. Liu, Z. Zhang, Y. Gao, and M. Wang, "Distributed target detection in subspace interference," *Signal Processing*, vol. 95, pp. 88–100, 2014.
- [4] L. Henriksen, "Real-time underwater object detection based on electrically scanned high-resolution sonar," in *Proceedings of IEEE Symp. Autonomous Underwater Vehicle Technology, AUV94, Cambridge, MA, USA*, Jul. 1994, pp. 99–104.
- [5] J. Zheng, T. Yang, H. Liu, T. Su, and L. Wan, "Accurate Detection and Localization of UAV Swarms-Enabled MEC System," *IEEE Transactions on Industrial Informatics*, pp. 1–1, 2020.
- [6] J. Liu, Y. Feng, D. Orlando, and H. Li, "Training data assisted anomaly detection of multi-pixel targets in hyperspectral imagery," *IEEE Transactions on Signal Processing*, vol. 68, pp. 3022–3032, 2020.
- [7] P. K. Hughes, "A High-Resolution Radar Detection Strategy," *IEEE Transactions on Aerospace and Electronic Systems*, vol. AES-19, no. 5, pp. 663–667, 1983.
- [8] X. Zhang, P. K. Willett, and Y. Bar-Shalom, "Monopulse radar detection and localization of multiple unresolved targets via joint bin processing," *IEEE Transactions on Signal Processing*, vol. 53, no. 4, pp. 1225–1236, Apr. 2005.
- [9] D. Orlando and G. Ricci, "Adaptive radar detection and localization of a point-like target," *IEEE Transactions on Signal Processing*, vol. 59, no. 9, pp. 4086–4096, Sep. 2011.
- [10] X. Tian, S. Zhang, and L. Peng, "Range cell migration correction for dim maneuvering target detection," in *Proceedings of the 2014 IEEE Radar Conference.*, May 2014, pp. 1247–1250.
- [11] J. Yang, X. Huang, T. Jin, T. John, and Z. Zhou, "New approach for SAR imaging of ground moving targets based on a Keystone transform," *IEEE Geoscience and Remote Sensing Letters*, vol. 8, no. 4, pp. 829–833, Jul. 2011.
- [12] C. Dai, X. Zhang, and J. Shi, "Range cell migration correction for bistatic SAR image formation," *IEEE Geoscience and Remote Sensing Letters*, vol. 9, no. 1, pp. 124–128, Jan. 2012.
- [13] X. Li, L. Kong, G. Cui, and W. Yi, "A fast detection method for maneuvering target in coherent radar," *IEEE Sensors Journal*, vol. 15, no. 11, pp. 6722–6729, Nov. 2015.
- [14] P. Addabbo, D. Orlando, and G. Ricci, "Adaptive radar detection of dim moving targets in presence of range migration," *IEEE Signal Processing Letters*, vol. 26, no. 10, pp. 1461–1465, Oct. 2019.
- [15] P. Stoica and Y. Selen, "Model-order selection: A review of information criterion rules," *IEEE Signal Processing Magazine*, vol. 21, no. 4, pp. 36–47, Jul. 2004.
- [16] E. Conte, A. De Maio, and G. Ricci, "GLRT-based adaptive detection algorithms for range-spread targets," *IEEE Transactions on Signal Processing*, vol. 49, no. 7, pp. 1336–1348, July 2001.
- [17] M. A. Richards, J. A. Scheer, and W. A. Holm, *Principles of Modern Radar: Basic Principles*. Raleigh, NC: Scitech Publishing, 2010.
- [18] H. L. Van Trees, *Optimum Array Processing (Detection, Estimation, and Modulation Theory, Part IV)*. John Wiley & Sons, 2002.
- [19] F. C. Robey, D. R. Fuhrmann, E. J. Kelly, and R. Nitzberg, "A CFAR adaptive matched filter detector," *IEEE Transactions on Aerospace and Electronic Systems*, vol. 28, no. 1, pp. 208–216, 1992.